

1 **Multiple equilibria in a cloud resolving model**

Sharon L. Sessions,¹ Satomi Sugaya,¹ David J. Raymond,¹ and Adam H.

Sobel²

David J. Raymond, Department of Physics and Geophysical Research Center, New Mexico Tech, 801 Leroy Place, Socorro, NM 87801, USA.

Sharon L. Sessions, Department of Physics and Geophysical Research Center, New Mexico Tech, 801 Leroy Place, Socorro, NM 87801, USA. (sessions@kestrel.nmt.edu)

Adam H. Sobel, Department of Applied Physics and Applied Mathematics, S.W. Mudd, Room 217, Columbia University, 500 West 120th Street, New York, NY 10027, USA.

Satomi Sugaya, Department of Physics, New Mexico Tech, 801 Leroy Place, Socorro, NM 87801, USA.

¹Department of Physics and Geophysical
Research Center, New Mexico Tech,
Socorro, New Mexico, USA.

²Department of Applied Physics and
Applied Mathematics and Earth and
Environmental Sciences, Columbia
University, New York, New York, USA.

2 **Abstract.** Multiple equilibria corresponding to either a state with per-
3 sistent, precipitating deep convection or a non-precipitating state are shown
4 to exist in a cloud resolving model employing the weak temperature gradi-
5 ent (WTG) approximation. WTG is important for the existence of both equi-
6 libria; numerical experiments show that a weak enforcement of WTG elim-
7 inates the dry non-precipitating state. In situations which support both equi-
8 libria, we find that the dry equilibrium has a small or negative gross moist
9 stability, while larger values correspond to the precipitating equilibrium.

1. Introduction

10 Recent work by *Sobel et al.* [2007, hereafter SBB07] has demonstrated the existence of
11 multiple equilibria in a single column model of the atmosphere using the weak temperature
12 gradient (WTG) approximation with parameterized deep convection. They showed that
13 in conditions with sufficient convective available potential energy (CAPE) for convection
14 to occur, an initially dry column would remain dry unless some mechanism (such as
15 horizontal moisture advection) sufficiently moistened the free troposphere. This work is
16 directly related to multiple equilibria of the Hadley circulation [*Bellon and Sobel, 2009*],
17 which suggests that understanding this phenomena in limited-domain simulations may be
18 important to understanding the interaction between convection and large-scale dynamics
19 in the tropics.

20 In this work, we pursue the idea that multiple equilibrium states may exist in the
21 atmosphere by performing numerical experiments with a cloud resolving model (CRM)
22 which interacts with the implicit large-scale circulations in a parameterized way via the
23 WTG approximation. We demonstrate that multiple equilibrium states do exist in our
24 model, but only under strict conditions which depend on surface fluxes (controlled by
25 either imposed surface winds or sea surface temperatures (SSTs)), domain size, and the
26 time scale with which the local vertical profiles of potential temperature relax to that of
27 the large scale environment. The equilibrium state which is realized by the model depends
28 on the initial moisture in the modeled domain, which is consistent with the results from
29 SBB07.

30 In addition to determining the conditions for the existence of multiple equilibria within
31 our model, we investigate the gross moist stabilities of the transient and steady states.
32 We find that the gross moist stability is a particularly important parameter not only for
33 diagnosing the environment in either equilibrium, but in characterizing the development
34 of deep convection.

35 Since the WTG approximation and gross moist stability are both important concepts
36 in this paper, we review these in the following subsections (1.1 and 1.2). Our numerical
37 experiments are described in section 2; results are presented in section 3. The role of
38 gross moist stability in the context of multiple equilibria is discussed in section 4. Finally,
39 section 5 includes a general discussion and summary.

1.1. WTG in the model

40 We run a version of the cloud resolving model very similar to that described in *Raymond*
41 *and Zeng* [2005, hereafter RZ05]. The model implements the WTG approximation as
42 described in RZ05, which is based on the original ideas of *Sobel and Bretherton* [2000,
43 hereafter SB00]. The basic premise of WTG is that the potential temperature in the
44 tropics tends to be horizontally homogeneous, and any buoyancy anomalies produced by
45 surface heat fluxes, latent heat release or radiation redistribute quickly by means of gravity
46 waves [*Bretherton and Smolarkiewicz*, 1989; *Mapes and Houze*, 1995]. This redistribution
47 maintains the horizontal homogeneity in the temperature profiles. In the model, this effect
48 is achieved by the imposition of a hypothetical vertical velocity, called the WTG velocity,
49 which produces vertical advection of potential temperature sufficient to counteract the
50 effects of heating.

51 As described in RZ05, the WTG velocity substantially modifies the evolution of con-
52 vection. In this work, the model does not impose a strict background profile of potential
53 temperature, but rather allows the instantaneous local profile to relax to a reference pro-
54 file equal to the assumed large scale mean. The relaxation time scale, t_θ , is modulated
55 by a sinusoidal vertical profile as described in RZ05. The resulting WTG velocity is de-
56 termined by this relaxation in the troposphere, and is linearly interpolated to zero in the
57 boundary layer. Physically, we interpret t_θ to be the amount of time it takes a gravity
58 wave to cross the modeled domain. Though we may set this time scale according to realis-
59 tic gravity wave speeds for a given domain size, we vary this parameter to investigate the
60 response of the modeled convection. Furthermore, we may think of this relaxation time
61 scale as a measure of the weak temperature gradient approximation: $t_\theta = 0$ corresponds
62 to strict enforcement of WTG (as was used in SB00 and SBB07) while $t_\theta = \infty$ turns off
63 WTG mode in the simulations and allows the model to evolve toward radiative convective
64 equilibrium. The tropical environment falls somewhere in between these two extremes,
65 depending on the time and space scales of interest.

66 The model used in these simulations prescribes only the potential temperature relax-
67 ation time. This parameter controls the corresponding WTG vertical velocity which
68 vertically advects moisture. Horizontal advection of moisture from the surrounding envi-
69 ronment is determined by assuming that the advecting velocity is purely divergent, so that
70 it can be computed self-consistently from the WTG vertical velocity using mass continuity
71 (RZ05). In SBB07, on the other hand, the time scale for horizontal advection of moisture
72 was specified a priori. This can be thought of as an assumption that the rotational com-
73 ponent of the advecting horizontal velocity is much larger than the divergent component,

74 so that the latter can be neglected and the horizontal advection of moisture is decoupled
 75 from the WTG vertical velocity. SBB07 showed that the existence of multiple equilibria
 76 is sensitive to the moisture relaxation, and thus an important question arises: Does the
 77 existence of multiple equilibria depend on relaxation of the vertical profile of potential
 78 temperature or moisture? Because the horizontal advection time scale is not specified
 79 externally here, but rather determined interactively from the WTG vertical velocity, we
 80 cannot disentangle these effects and thus we do not address this question in the present
 81 study.

1.2. Normalized gross moist stability

82 The gross moist stability can be thought of as a measure of precipitation efficiency. It
 83 was first introduced in 1987 by *Neelin and Held* as a means to model tropical conver-
 84 gence based on the moist static energy budget (moist static energy being approximately
 85 conserved in moist processes). In this work, we choose to use the convention of *Ray-*
 86 *mond et al.* [2007], which defines the normalized gross moist stability (NGMS) in terms
 87 of moist entropy (which is also approximately conserved in moist convective processes).
 88 Specifically, we define Γ to be the NGMS:

$$89 \quad \Gamma = \frac{T_R[\nabla \cdot (s\mathbf{v})]}{-L[\nabla \cdot (r\mathbf{v})]} = \frac{T_R \frac{1}{g} \int \nabla \cdot (s\mathbf{v}) dp}{-L \frac{1}{g} \int \nabla \cdot (r\mathbf{v}) dp} \quad , \quad (1)$$

90 where s is the moist entropy, r is the total cloud water mixing ratio, and \mathbf{v} is the horizontal
 91 wind. The square brackets indicate a vertical pressure integral over the troposphere, g is
 92 the gravitational acceleration, and ∇ is the horizontal divergence operator. T_R and L are
 93 a constant reference temperature and the latent heat of condensation, which are included
 94 so that Γ is dimensionless. We thus define NGMS as the ratio of lateral moist entropy

95 export to moisture import. In a majority of cases, NGMS is a positive quantity, but can
 96 become negative if moist entropy and moisture are both imported into (or exported from)
 97 a convecting region.

98 Observations suggest that the sign of NGMS in a convecting region is related to the
 99 level of non-divergence in the horizontally averaged circulation [*López and Raymond, 2005;*
 100 *Back and Bretherton, 2006*]. In particular, when convergence is concentrated at low levels,
 101 as expected in the early stages of the development of deep convection, a vertical pressure
 102 integral of moist entropy or moist static energy divergence gives a net *import* of these
 103 quantities. Coupled with the moisture convergence, this results in a negative NGMS. In
 104 a region of subsidence, we expect moisture export, and either a modest import or export
 105 of moist entropy. The latter also results in a negative NGMS. As we will show in section
 106 4, both of these situations are realized in our model.

107 A thorough discussion on the role of NGMS in tropical dynamics can be found in
 108 *Raymond et al. [2009]*. As in *Raymond et al. [2007]*, the net precipitation in the steady
 109 state is related to the NGMS according to:

$$110 \quad P - E = \frac{T_R(F_s - R)}{L\Gamma} \quad , \quad (2)$$

111 where P is the precipitation rate, E is the surface evaporation rate, F_s is the surface
 112 moist entropy flux due to surface heat and moisture fluxes, and R is the pressure integral
 113 of the entropy sink per unit mass due to radiation divided by the acceleration of gravity.
 114 Equation (2) suggests that the net precipitation ($P - E$) is inversely proportional to
 115 the NGMS for a given net entropy forcing. This is consistent with the results from
 116 *Raymond and Sessions [2007]*, which showed that thermodynamic profiles which are either
 117 moister or more unstable at low levels result in smaller values of NGMS and increased

118 precipitation rates. The results described in section 4 are consistent with those findings,
119 and demonstrate that NGMS can be used as a diagnostic for characterizing the equilibrium
120 state of the system.

2. Experiments

121 For the implementation of the WTG approximation, we must specify the vertical pro-
122 files of potential temperature and mixing ratio representing the large-scale environmental
123 mean. For simplicity, we take this *reference profile* to be one of radiative convective equi-
124 librium (RCE), generated by averaging the last 3×10^6 s (≈ 35 days) in a 5×10^6 s (\approx
125 58 day) non-WTG simulation (i.e., $t_\theta = \infty$). RCE profiles are generated with imposed
126 horizontal surface wind speeds of 5 ms^{-1} over tropical oceans with SSTs of 303 K. The
127 horizontal wind is perpendicular to the two-dimensional plane of the domain (all simula-
128 tions are in 2D to decrease the computational demand). The simple radiative model used
129 in *Raymond and Zeng* [2000] calculates radiative cooling interactively in these simulations.

130 We have found that the RCE profiles are sensitive to the domain size and we thus
131 perform RCE simulations for each domain size and grid resolution used in the numerical
132 experiments. The vertical domain size used in the experiments is 20 km with a 250 m
133 vertical resolution. We used horizontal domain sizes of 50, 100 or 200 km. The 100 and
134 200 km domains had a horizontal resolution of 1 km (to reduce computational expense).
135 Most of the 50 km domains used a horizontal grid resolution of 500 m, though several
136 experiments used a 1 km grid to facilitate comparisons with the larger domains. Unless
137 otherwise noted, all references to the 50 km domain correspond to runs with a 500 m
138 resolution.

139 Figures 1A and 1B show a comparison between the horizontal and temporal averages
140 of potential temperature and mixing ratio of the RCE simulations. To emphasize the
141 differences, we plot the deviations of all profiles from the 50 km domain size with 500
142 m resolution. The differences between the logarithm of the mixing ratios is shown in
143 figure 1C to exaggerate the differences in the moisture content of the upper troposphere.
144 The solid lines correspond to 50 km domains with line thickness indicating grid resolution
145 (thin and thick lines corresponds to 500 m and 1 km resolution, respectively). Dashed and
146 dotted lines show deviations of the 100 km and 200 km domains from the 50 km domain.
147 Note that the larger domains are slightly warmer and dryer in the free troposphere (from
148 about 2.5-12 km; figures 1A,B) than the 50 km domains, though the 50 km domain with
149 coarser resolution is considerably dryer in the boundary layer.

150 We can understand the origin of these differences by comparing the fractional cover-
151 age of precipitating clouds for the different RCE simulations. Comparing the effects of
152 grid resolution on the 50 km domains, we find that the finer grid produces a consider-
153 ably moister domain with precipitating clouds covering a larger fraction of the space-time
154 domain (18.5% versus 14.7% of the domain has a precipitation rate of at least 1 mm
155 day⁻¹). The larger domains have a slightly lower fractional coverage (13.2% and 13.1%
156 with precipitation rate of at least 1 mm day⁻¹ for the 100 and 200 km domains, respec-
157 tively), which suggests that there is more room for descent to exist. This in turn allows
158 the domain to warm and dry slightly compared to the smaller domains. In section 3, we
159 show that the differences in the RCE reference profiles have essentially no effect on the
160 WTG runs with 1 km grid resolution, but that the moister profile associated with the
161 finer resolution produces slightly higher precipitation rates (e.g., see figures 3 and 4).

162 Having specified the reference profile for the WTG simulations, we now describe the
 163 parameters in the modeled domain. We choose to fix the sea surface temperature at 303 K,
 164 and vary the strength of the surface horizontal wind. For each experiment, the wind speed
 165 is specified and approximately maintained throughout the duration of the simulation.
 166 Both SST and surface winds control surface fluxes, with larger values producing more
 167 convection and correspondingly greater precipitation rates (e.g., RZ05 and SBB07). In
 168 these experiments, the prescribed surface wind ranges from 0-20 ms^{-1} , with most runs set
 169 at 5, 7, 10 or 15 ms^{-1} .

170 As discussed in section 1.1, we also vary the time scale of relaxation of potential tem-
 171 perature toward the large-scale mean. This effectively controls the degree to which the
 172 model obeys the WTG approximation, and consequently controls the magnitude of the
 173 WTG vertical velocity. By mass continuity, this fixes the horizontal flow and controls the
 174 horizontal advection of moisture from the surrounding environment.

175 Each experiment is initiated with vertical profiles of potential temperature and total
 176 water mixing ratio which may differ from the RCE reference profile. The initial mixing
 177 ratio profile is taken to be

$$178 \quad r_{t(\text{init})}(z) = f r_{t0}(z) \quad , \quad (3)$$

179 where $r_{t0}(z)$ is the RCE profile which represents the surrounding environment, and f is
 180 a fractional multiplier ($0 \leq f \leq 1$). Initializing the domain with the moisture content
 181 of the surrounding environment corresponds to $f = 1$, while a domain that is initially
 182 completely dry has $f = 0$. $f = 0, 1$ correspond to the initial conditions used in SBB07.
 183 In addition to these extremes, we perform some experiments with the initial moisture of
 184 the modeled domain as some fraction of the RCE profile ($0 < f < 1$).

185 The initial potential temperature profile is given by

$$186 \quad \theta_{init} = \theta_0(1 + \delta\theta_{local}/\theta_0)(1 + \delta\theta_{random}/\theta_0) \quad , \quad (4)$$

187 where θ_0 is the RCE profile used to represent the large scale mean, $\delta\theta_{local}$ and $\delta\theta_{random}$
188 represent localized and random perturbations respectively:

$$189 \quad \begin{aligned} \delta\theta_{local} &= \delta\theta_{local}^{max} \exp[-(x_s^2 + z_s^2)] \\ \delta\theta_{random} &= \delta\theta_{random}^{max} z_s \exp[1 - z_s] \end{aligned} \quad . \quad (5)$$

190 Here, $\delta\theta_{local}^{max}$ and $\delta\theta_{random}^{max}$ are maximum values of the respective perturbations, and x_s
191 and z_s are scaled Cartesian coordinates (i.e., $z_s = z/z_{scale}$, where z_{scale} defines the width
192 of the localized Gaussian perturbation; an analogous definition holds for x_s). For most
193 simulations, $x_{scale} = 3$ km, $z_{scale} = 1$ km. Random temperature fluctuations with a
194 maximum magnitude¹ of $\delta\theta_{random}^{max} = 0.3$ K are distributed at 1 km in altitude. Similarly,
195 we set $\delta\theta_{local}^{max} = 9$ K to prescribe a localized temperature increase for a 3 km region
196 centered horizontally with a vertical extent of about 1 km centered at 1 km in altitude.
197 We originally chose such a large perturbation in hopes that we could get a reliable response
198 (either developing precipitation or not) from an initially dry domain. A limited number of
199 simulations which vary $\delta\theta_{local}^{max}$ and $\delta\theta_{random}^{max}$ were performed to determine the sensitivity to
200 initial conditions. Preliminary results suggest that the final state of the system does not
201 seem to be very sensitive to these perturbations, though more investigation is necessary in
202 order to determine this conclusively. We do note, however, that setting $\delta\theta_{random}^{max} = \delta\theta_{local}^{max} =$
203 0 and $f = 0$ will not generate convection no matter what the boundary conditions are.

204 One of the primary goals of this paper is to characterize the statistically steady states
205 of the system, which we assume with some confidence will remain stable indefinitely. The
206 steady state precipitation and NGMS are taken as averages over the last month of the

simulation. In most cases, the simulation was run for 4 months, though the run time varied from 60 to 364 days². The shorter runs were justified from the observation that once the model began precipitating, it equilibrated rather quickly (over a period of hours), and remained in a statistically steady state. For the numerical experiments which were initially dry, it could take several days or months to develop precipitation (in one case, this transition occurred after 70 days, see figure 2). In those cases, longer run times may be necessary to observe a transition. For that reason, several experiments were run for a full year to verify whether the system would transition at a later time or if it was truly in a stable equilibrium. Of these, most remained completely dry for the duration of the model run. Two experiments showed moistening of the troposphere after 4 months which was insufficient to overcome convective inhibition and trigger deep convection, even after running the simulation for a full year. In these cases, the precipitation rate remained negligible compared to the corresponding rate in the equilibrium state with persistent deep convection, although the NGMS remained noisy up until the last month of the simulation. Repeating these experiments with slightly different initial conditions (i.e., adjusting $\delta\theta_{local}$ and $\delta\theta_{random}$) allowed the model to equilibrate quicker, but did not change the final state of the system.

Finally, we note that despite some model runs of up to one year, we cannot exclude the possibility that convection could still develop after the model run time. Indeed, of the initially dry experiments which eventually precipitated, we found that the amount of time it took to initiate precipitation increased with decreasing surface wind speeds and potential temperature relaxation time. This is shown in figure 2. On the left, the amount of time it took for a precipitation rate of at least 1 mm day^{-1} to develop is plotted as a

function of the relaxation rate (t_{θ}^{-1}) for different surface wind speeds and domain sizes. In all but one instance, the time to precipitate increased with decreasing t_{θ} , suggesting that a further decrease in t_{θ} (which corresponds to a stricter enforcement of WTG) would require a longer wait time to transition to the precipitating equilibrium for a given domain size and wind speed. Considering that the real atmosphere will not maintain steady conditions over a time scale of months, we do not give further consideration to this possibility. Also note that surface fluxes play a role in the amount of time required for precipitation to occur. As shown on the right panel of figure 2, more vigorous surface fluxes associated with higher surface wind speeds initiate convection more quickly. In this case, if we consider wind speeds close to or below the values used to compute the RCE reference profile, we do not expect convection to initiate no matter how long we wait, since there will not be sufficient CAPE. The choice of a 4 month simulation is somewhat arbitrary, and is chosen in hopes that this gives initially dry atmospheres enough time to develop convection if they are going to do so, without excessive computation time.

3. Results

As in SBB07, we perform parallel experiments with the domain initialized either with the moisture profile of the surrounding environment or completely dry. We then vary the boundary conditions (surface wind speed, domain size and WTG relaxation time) in each case to establish the range of conditions which support multiple equilibria. Upon establishing this range, we vary the initial conditions to determine the sensitivity of the realized equilibrium to the initial state of the domain. The results from SBB07 suggest that the final equilibrium state depends on the initial moisture in the modeled domain. We cannot say a priori whether or not the system always evolves to the precipitating

252 equilibrium state if *some* amount of moisture exists in the free troposphere, or if there is
253 a minimum amount required to overcome convective inhibition. We address this issue in
254 this section, as well as how this depends on the boundary conditions.

255 In addition to determining the range of boundary conditions which support multiple
256 equilibria, and the sensitivity of the final state to initial conditions, we consider the NGMS
257 as a diagnostic for characterizing the equilibrium state of a modeled domain. Furthermore,
258 we discuss the role of NGMS in developing (or decaying) convection as well as in the steady
259 state. These results are shown in section 4.

3.1. Dependence on surface wind speed

260 The first set of experiments aims to determine the range of wind speeds which support
261 multiple equilibria for a given domain size and potential temperature relaxation time
262 (with SST fixed). Figure 3 shows results for a 50 km domain with $t_\theta = 1.85$ hours.
263 Experiments initiated with RCE moisture profiles are indicated by circles (solid line),
264 while squares (dashed line) represent initially dry experiments. Thin lines correspond to
265 a grid resolution of 500 m, while thick lines give the 1 km grid results. This figure is
266 analogous to figure 2 in SBB07, except in SBB07, the wind speed was fixed and SSTs
267 were varied compared to the RCE value. As discussed in section 2, both have the effect
268 of modulating surface fluxes.

269 From figure 3 (top), we note that a single, precipitating equilibrium exists for wind
270 speeds of 12 ms^{-1} and greater, regardless of horizontal grid resolution. For the finer (500
271 m) grid, a single non-precipitating equilibrium exists below a wind speed of 5 ms^{-1} , while
272 horizontal wind speeds from 5 to 10 ms^{-1} can sustain either a dry or a precipitating
273 steady state, depending on the initial moisture profile. Specifically, in the range of wind

274 speeds that can sustain multiple equilibria, an initially dry domain will remain dry, while
275 a pre-moistened domain will sustain persistent convection. The only difference in the
276 simulations is the initial mixing ratio profile, which is consistent with results of SBB07.
277 Similar results also hold for the coarser (1 km) grid, though multiple equilibria persist
278 even for wind speeds as low as 3 ms^{-1} .

279 These results demonstrate that multiple equilibrium states exist under certain boundary
280 conditions in our CRM in the WTG approximation. As the wind speed is increased,
281 surface fluxes overcome convective inhibition, allowing shallow convection to penetrate
282 into the free troposphere thus effectively destroying the dry equilibrium state. The bottom
283 panel of figure 3 shows the steady state value of NGMS for the corresponding runs. The
284 significance of these values will be discussed further in section 4.2.

285 Experiments similar to those presented in figure 3 on 100 and 200 km domains show
286 similar behavior, with one important distinction: The larger the domain, the smaller
287 the range in which multiple equilibria exist. Figure 4 shows that with a thermodynamic
288 relaxation time of 1.85 hours, there is only a very narrow range of wind speeds which
289 permit multiple equilibrium on a 100 km domain, and this range decreases even more for
290 a computational domain of 200 km. Also note that, unlike the coarsely gridded 50 km
291 domain, the precipitating equilibrium is destroyed for wind speeds less than 5 ms^{-1} . We
292 discuss the dependence on domain size below.

3.2. Dependence on domain size and relaxation time

293 We did not systematically probe the dependence of precipitation rate on domain size
294 for different relaxation rates, but in comparable instances, we found very little difference
295 in the domain averaged precipitation rate in any of the domains with 1 km horizontal grid

296 resolution and wind speeds of 5 ms^{-1} and greater (as discussed above, wind speed less
 297 than this sustained precipitation in the 50 km domain while other domain sizes dried and
 298 remained dry). Furthermore, there is only a slight difference between the results from a
 299 1 km grid and the 500 m grid, with the finer grid producing slightly higher precipitation
 300 rates (compare figures 3 and 4). As explained in section 2, we suspect that this difference
 301 is attributed to the moister RCE reference profile generated with a finer grid resolution.
 302 Accounting for this, we conclude that in the convecting equilibrium state, there is little
 303 dependence of precipitation rate on domain size for a given wind speed and potential
 304 temperature relaxation time.

305 Though the change in precipitation rate as a function of domain size in the precipitating
 306 equilibrium is nearly negligible, the role of domain size in determining the existence of
 307 multiple equilibria (as seen in figure 4) is quite significant. Smaller computational domains
 308 allow multiple equilibria over a larger range of wind speeds. This dependence on domain
 309 size is at least partially related to the distribution of convective inhibition in the modeled
 310 domain. Figure 5 shows a histogram of deep convective inhibition [DCIN, *Raymond et al.*
 311 2003], where DCIN is defined as

$$312 \quad DCIN = s_t - s_b \quad . \quad (6)$$

313 Here, s_t is the threshold entropy for convection and is defined as the vertical average of
 314 the saturated moist entropy over the height range 1750-2000 m; s_b is the boundary layer
 315 entropy defined as the average of moist entropy over 0-1000 m. The curves on the right
 316 correspond to simulations which were initiated with dry mixing ratio profiles ($f = 0$ from
 317 equation 3), while curves on the left correspond to simulations initiated with the RCE
 318 mixing ratio profiles ($f = 1$). For this set of boundary conditions, all simulations which

319 were initially dry remained dry, and the values of DCIN were taken from the last month
320 and over the entire domain of each simulation (the number of occurrences was normalized
321 to account for a larger number of grid points on larger domain sizes). Even in runs which
322 remained dry, the 200 km domain experienced a higher frequency of lower values of DCIN,
323 which increases the possibility that convection will spontaneously initiate. Indeed, this
324 does occur when the surface wind speed is increased from 5 to 7 ms^{-1} (see, e.g. figure
325 4). The lower values of convective inhibition may be a result of larger, more developed
326 circulations permitted by the larger domains. Though we believe that this contributes to
327 the dependence of multiple equilibria on domain size, the similarity between the DCIN
328 distributions in the 50 km and 100 km domains suggests that this is not the whole story.

329 The results from SBB07 showed that the existence of multiple equilibrium states de-
330 pends on the time scale of horizontal moisture advection. As we explained earlier, our
331 model ties moisture advection to the time scale of the potential temperature relaxation in
332 the WTG implementation via mass continuity. To explore the implications of this relation,
333 we performed several experiments to determine the sensitivity of multiple equilibria with
334 respect to the WTG potential temperature relaxation time, t_θ . Decreasing the value of t_θ
335 is tantamount to decreasing the amount of time it takes to remove buoyancy anomalies in
336 the vertical profile of potential temperature. A relaxation time of zero corresponds to an
337 instantaneous relaxation to the specified environmental profile, and thus strictly enforces
338 the WTG approximation. Increasing t_θ lengthens the relaxation time, and $t_\theta = \infty$ turns
339 off WTG since the relaxation to the background profile takes infinitely long.

340 Figure 6 illustrates the dependence of the final precipitation state on the potential tem-
341 perature relaxation time for the different domain sizes. All of the experiments shown

342 were initiated with zero moisture and have an imposed horizontal wind speed of 10 ms^{-1} .
343 The larger values of t_θ result in a precipitating state, and all domain sizes can main-
344 tain a dry equilibrium for sufficiently small t_θ . This means that the more strongly the
345 WTG approximation is enforced, the more likely the system is to sustain multiple equi-
346 libria. Furthermore, the relaxation time scale at which the dry equilibrium is destroyed
347 decreases with increasing domain size. This implies that the WTG approximation must
348 be more vigorously enforced the larger the domain in order to maintain multiple equi-
349 libria. To rationalize this tendency, consider that smaller relaxation times prevent the
350 development of domain-averaged temperature profiles which differ significantly from that
351 of the reference profile (see figure 8 and the discussion below). Perhaps such temperature
352 profile anomalies are more conducive to the development of deep convection. It may also
353 be that larger domains are more able to take advantage of these anomalies by producing
354 circulations in the domain of larger horizontal scale. Presumably in the presence of radia-
355 tive cooling, if there is no convection and t_θ is finite, the troposphere cools which increases
356 CAPE and decreases convective inhibition, resulting in a more favorable environment for
357 convection.

358 Figure 7 encapsulates the dependence of multiple equilibria on domain size and poten-
359 tial temperature relaxation time for given surface flux conditions. All symbols represent
360 experiments which were initiated with completely dry profiles. Solid circles represent
361 simulations which eventually precipitated while open squares indicate that the domain
362 remained dry. This shows that precipitation is more likely to develop with longer re-
363 laxation times or larger domains. Furthermore, this type of figure shows the range of

364 parameters under which our model supports multiple equilibria since we can conclude
365 that the dry equilibrium is destroyed under the conditions which developed precipitation.

366 We now discuss the interpretation of t_θ as a measure of the WTG approximation, and
367 the relationship between t_θ and precipitation rate. An inspection of the vertical profile of
368 potential temperature in the steady state suggests a nearly constant deviation from the
369 reference profile in the free troposphere (not shown). Taking the free troposphere to be
370 between 4 km and 12 km, we define $\delta\theta$ to be the vertical average over this height range,
371 the horizontal average over the model domain, and the time average over the last month
372 of the simulation. Figure 8 shows a plot of $\delta\theta$ as a function of t_θ for simulations with
373 all ranges of surface wind speeds, all domain sizes, and arbitrary initial moisture. The
374 black filled triangles represent the simulations which converged to the dry equilibrium,
375 independent of model parameters, while all other symbols represent simulations which
376 eventually sustained precipitation and are coded to indicate wind speed. There are several
377 observations we can make from this figure. First note that strong convection (i.e., when
378 convective heating is greater than radiative cooling) corresponds to $\delta\theta > 0$, with stronger
379 heating resulting in larger temperature deviations (indicated by steeper slopes in figure
380 8). Weak or non-existent convection results in $\delta\theta < 0$. The WTG formulation of the
381 temperature basically guarantees this behavior; Since we parameterize the large-scale
382 vertical advection as a relaxation (measured by t_θ), it responds to the tendencies given by
383 radiation and convection, which implies that those control the sign of $\delta\theta$. So here we see
384 how convection controls the temperature anomalies. However, the temperature anomalies
385 are also known to influence convection (see e.g., *Raymond and Sessions* [2007]), which
386 implies a tight coupling between the two.

387 To see how the coupling between convection and temperature anomalies influence pre-
388 cipitation rate as we vary t_θ , we plot precipitation rate versus $\delta\theta$ for all experiments
389 (shown in figure 9). Again we see that negative temperature deviations correspond ei-
390 ther to the dry equilibrium (precipitation rate is zero) or to cases where convection is
391 weak (as when the surface wind speed is equal to the ambient RCE value, in this case 5
392 ms^{-1}). Stronger convection associated with positive $\delta\theta$ have non-zero precipitation rates.
393 Note that for a given surface wind speed, there is an increase in precipitation rate as the
394 WTG approximation is relaxed (t_θ and $\delta\theta$ increase proportionally from zero), followed by
395 a subsequent decrease. The rise corresponds to a switch from the dry equilibrium to the
396 precipitating one, while the fall corresponds to the slower shift from a WTG-dominated
397 simulation to one approaching RCE (as $t_\theta \rightarrow \infty$). This behavior emphasizes the coupling
398 between the atmospheric stability and precipitation.

3.3. Dependence on initial conditions

399 So far we have confirmed the existence of multiple equilibria in our CRM using the WTG
400 approximation, and determined the range of parameters which may sustain both states.
401 Given a specific set of boundary conditions that may sustain both equilibria, we find that
402 the state which is ultimately realized by the model depends on the initial moisture profile
403 of the modeled domain. This is identical to the conclusions in SBB07. SBB07 suggested
404 that the persistence of the dry equilibrium in the presence of positive CAPE requires that
405 the free troposphere be able to remain completely dry, even over a moist boundary layer.
406 Though not shown, all experiments which remained dry observed this condition.

407 To further test the sensitivity of the final equilibrium state to the initial moisture, we
408 performed a series of experiments which were initiated with a mixing ratio profile equal

409 to a non-zero fraction of the reference profile. We find that there is a minimum amount
410 of moisture necessary to move the system from the non-precipitating to the precipitating
411 equilibrium state. An example of this is shown in figure 10. Here, each bullet represents
412 a simulation performed on a 50 km domain with $t_\theta = 17$ min. Line styles and symbols
413 indicate different wind speeds. The initial moisture is taken to be a fraction of the RCE
414 mixing ratio profile (with the fraction given by f in equation (3)). These results show that
415 even though some simulations are initiated with non-zero moisture in the troposphere, the
416 amount is insufficient to initiate deep convection and transition to the precipitating equi-
417 librium. The larger the surface fluxes, the more likely a small amount of moisture will
418 result in persistent deep convection. However, domains with low surface winds may toler-
419 ate a relatively large fraction of moisture without initiating deep convection. For example,
420 one experiment with a wind speed of 7 ms^{-1} remained dry even with an initial moisture
421 profile equal to 80% of the moisture of the surrounding environment. In this particular
422 case, the initial moisture in the free troposphere rapidly vanishes due to subsidence and
423 lateral export, which can be deduced from figures 11 and 12.

424 Figure 11 shows the evolution of relative humidity for the 7 ms^{-1} experiment initialized
425 with 80% of the reference moisture profile (white is zero relative humidity, while black
426 indicates 100%). All of the initial moisture in the free troposphere is gone by day 15.
427 Figure 12 shows the corresponding profile of vertical mass flux for the first 10 days. Each
428 profile represents an average of the entire day. Initially, there is subsidence throughout
429 the entire troposphere, with a maximum downdraft at 12 km. Subsequent days acquire
430 a small updraft in the boundary layer with a maximum at day 4. Together with the
431 downdraft in the free troposphere, this suggests a thin horizontal outflow at the level of

432 zero mass flux (just above 1 km). Physically, this corresponds to shallow non-precipitating
433 clouds mixing boundary layer air with air aloft and detraining air near cloud base, similar
434 to the process described by *Raymond and Blyth* [1996]. In the model it is effected by the
435 subgrid mixing process rather than by explicit convection. This mixing process removes
436 the moisture from the free troposphere, and by day 9, the system is completely subsiding.
437 Once the moisture in the free troposphere has been evacuated, the boundary layer also
438 becomes unsaturated, though it remains moist in the steady state. The mass flux profile
439 changes very little from the last day plotted in this figure. From this we conclude that
440 the mass convergence in the boundary layer is too weak to overcome convective inhibition
441 and the troposphere dries and remains dry.

442 Though the initial moisture in the troposphere will ultimately determine which equilib-
443 rium state is realized, the boundary conditions (surface wind speeds, SST, domain size and
444 relaxation time scale in WTG mode) will determine whether there are multiple equilibria.

4. NGMS as a diagnostic

445 For conditions which support multiple equilibria, we have shown that the equilibrium
446 state that is ultimately realized depends on the initial moisture in the troposphere. In
447 some cases, a dry equilibrium is sustained even with small but non-zero initial moisture,
448 while in others, just a slight amount of moisture will move the system to the precipitating
449 equilibrium. The amount of moisture tolerated depends on the other model parameters
450 (surface wind speed, domain size and time to relax potential temperature profile to the
451 large scale mean). Given that identical boundary conditions may sustain deep convection
452 or not, it is desirable to characterize the environment with a variable capable of diagnosing
453 the respective equilibrium. Below, we consider the NGMS as a candidate for this purpose.

454 *Raymond et al.* [2009] discussed the role of NGMS in transient flows as well as in a
455 multiple equilibrium situation. We can address both of these situations from the results of
456 our numerical experiments. Of particular interest is the possibility of a negative NGMS,
457 which is closely related to the existence of a dry equilibrium in the steady state.

4.1. NGMS in transient flows

458 The nature of the experiments reported here provides an opportunity to consider sit-
459 uations which make a definite transition from a dry to precipitating state or vice versa.
460 The former case is encountered in an initially dry atmosphere in which the troposphere
461 proceeds to moisten and the system initiates and sustains deep convection. During such
462 an evolution, the initial convective vertical mass flux profile typically has a maximum at
463 lower levels [*Sobel, 2007*]. By mass continuity, this suggests that the mass convergence is
464 concentrated near the surface, where the moist entropy is greater than at middle levels
465 [*Raymond et al., 2009*]. Alternatively, the radiative cooling profile can cause a net inflow
466 at high levels where moist entropy is large compared to mid-levels (this happens in our
467 simulations, see e.g., figure 14). A vertical pressure integral under either of these condi-
468 tions results in a a net import of moist entropy. Furthermore, moisture is likely to be
469 imported under such conditions, which implies a period where the system has negative
470 NGMS. An example of the transition from a dry state to a precipitating one is shown
471 in figure 13. Here, the saturation fraction increases gradually, with a sharp increase be-
472 ginning after about 24 days of the simulation which triggers the onset of precipitation.
473 At this time, a change in the implicit large-scale divergence profile associated with the
474 convective heating causes the descent in the lower free troposphere to weaken, which in
475 turn causes the net moisture convergence ($-\nabla \cdot r\mathbf{v}$) to go from negative to positive.

476 Consequently, the NGMS (see eq. (1)) goes from large and positive to large and nega-
477 tive. For a period of about 2.5 days, the domain is *importing* both moisture and moist
478 entropy. When the system begins to export moist entropy ($[\nabla \cdot s\mathbf{v}]$ goes from negative to
479 positive), the saturation fraction and precipitation rate level off. In this case, the steady
480 state is exporting moist entropy, importing moisture, resulting in a positive NGMS in the
481 precipitating equilibrium.

482 Figure 14 shows the evolution of the vertical mass flux (left) and moist entropy (right) for
483 days 22-27 of the simulation, during which the domain makes the transition from the dry to
484 the precipitating state. This progression begins with a descent throughout the troposphere
485 with a maximum near 2 km and small updraft near the surface, indicating detrainment
486 just above 1 km in height. At this time, moisture is being exported from the domain,
487 and there is a net import of moist entropy due to the circulation near the surface. During
488 the period with negative NGMS (days 24-25), there is very little average vertical motion
489 in the free troposphere (which indicates the existence of some convective updrafts, whose
490 condensation heating balances radiative cooling), and the low level downdraft decays
491 which weakens the divergence near the surface, allowing moisture from the boundary layer
492 to penetrate into the free troposphere. On day 25, levels of convergence (surface, 9 km
493 altitude) import higher values of moist entropy than exported at the levels of divergence
494 (4 km), thus maintaining the import of moist entropy. By day 26, there is upward vertical
495 motion from the surface to the tropopause, which progresses to strong convergence near
496 2.5 km. The final stages produce a net export of moist entropy (and $\text{NGMS} > 0$).

497 In addition to convection developing in a quiescent region, negative NGMS can also
498 occur in decaying convection as might be expected with entrainment of dry air as in

499 *Sobel and Bellon* [2008]. In our simulations, this could happen for instance if a system
500 is initiated with a moisture profile representative of the surrounding environment, but
501 with surface wind speeds less than the value used for calculating RCE, or if the initiated
502 moisture is insufficient to sustain convection (as in the case shown in figures 11 and 12).
503 Figure 15 is an example of the first possibility. In this case, we see moisture is exported
504 from the tropospheric column; rainfall rate³ drops along with the saturation fraction, and
505 NGMS is negative until the domain begins to export moisture. At day 11, moist entropy is
506 exported for a period of about 3 days, again resulting in a negative NGMS. In the steady
507 state, the system is exporting moisture and importing moist entropy, resulting in a positive
508 NGMS. The evolution of mass flux and domain averaged moist entropy for the first 16
509 days of this simulation is shown in figure 16. Times where moisture and moist entropy
510 are imported/exported are emphasized along with the corresponding sign of NGMS. An
511 interesting observation from this time sequence is that the atmosphere near the surface
512 is close to saturation for times when the lateral export of moist entropy is increasing; as
513 this quantity decreases, the atmosphere just above the surface becomes unsaturated. This
514 implies that the surface fluxes are responsible for the negative NGMS during days 11-17.

515 So we see in both developing and decaying stages of deep convection, NGMS may
516 become negative.

517 The sign of NGMS in the transient stages of convection is particularly salient with
518 respect to observations reported by *López and Raymond* [2005] and *Back and Bretherton*
519 [2006]. *Back and Bretherton* considered the moist static energy budget (an alternative
520 to moist entropy), and found that the sign of moist static energy was determined by
521 the strength of the contribution due to horizontal motions in comparison to the vertical

522 contribution. In the east Pacific, vertical advection contributed a negative value of moist
523 static energy, while in the west Pacific the contribution was positive. In both regions, the
524 contribution to the moist static energy by horizontal motions was positive. The sum of
525 the horizontal and vertical contributions in the east Pacific was found to be either positive
526 or negative, depending on the relative contributions by horizontal motions. Both *Back*
527 *and Bretherton* [2006] and *López and Raymond* [2005] conclude that import or export of
528 thermodynamic quantities (which contribute to the sign of NGMS) are determined by the
529 shape of the vertical motion profile. Our results support these conclusions.

4.2. NGMS in steady state

530 Now we consider the steady state NGMS as a diagnostic for characterizing the equilib-
531 rium state. For example, figure 3 compares the steady state values of NGMS for the two
532 equilibrium states for the 50 km domains (500 m and 1 km grid resolutions). In the case
533 where a single equilibrium exists (either dry or precipitating), the steady state NGMS is
534 the same for both sets of experiments, independent of the initial moisture profile. In the
535 range of wind speeds where both equilibria exist, the value of NGMS for the precipitating
536 state is considerably larger than that of the dry state, and we can see that NGMS provides
537 a valuable characterization of the environmental flows. Note that the value of NGMS for
538 a surface wind speed of 5 ms^{-1} is either very large or very small for the precipitating
539 equilibrium, depending on grid resolution (figure 3). We know that RCE is a possible
540 solution for these boundary conditions, so we might expect the WTG model to reach
541 that solution. In that case, NGMS would be undefined since there is already a balance
542 in moisture and moist entropy, and a time average of the entrainment or detrainment of
543 these quantities should be close to zero and their ratio undefined. However, that need

544 not occur exactly, so instead we see large fluctuations in NGMS at this wind speed. For
545 this reason, we exclude calculations of NGMS in WTG simulations with surface winds of
546 5 ms^{-1} (or, more generally, under RCE boundary conditions). For wind speeds greater
547 than or less than 5 ms^{-1} , either convective updrafts or subsidence dominates, which im-
548 plies non-zero averages of moisture and moist entropy convergence⁴. Thus, for non-RCE
549 boundary conditions, a time average of NGMS is useful (and we emphasize that the time
550 average is performed *before* the ratio of entropy divergence to moisture convergence is
551 taken).

552 To further demonstrate the value of NGMS as a diagnostic, figure 17 shows a scatter
553 plot of precipitation rate as a function of NGMS for all experiments with surface winds
554 greater than 5 ms^{-1} . Those with surface winds of 5 ms^{-1} are excluded since there is
555 essentially no correlation between the time average of NGMS and precipitation for the
556 reason discussed above. The experiments with wind speeds less than 5 ms^{-1} are dry in
557 the steady state, with NGMS values less than 0.25. The symbols indicate the prescribed
558 surface wind speed in the particular experiment. Each symbol represents the steady state
559 rain rate and NGMS, independent of the initial moisture and domain size. There are
560 three striking observations from figure 17. First, *all* simulations which resulted in a dry
561 equilibrium have an NGMS less than 0.25, while those in the convecting equilibrium state
562 have an NGMS greater than 0.35. A vertical line corresponding to $\Gamma = 0.3$ clearly divides
563 the precipitating and dry equilibria.

564 The sharp transition in NGMS for the precipitating versus non-precipitating equilibrium
565 states could be related to the *Peters and Neelin* [2007; also *Neelin et al.*, 2009] hypothesis
566 that the tropical atmosphere represents an observable example of self-organized criticality.

567 Though further work is necessary to verify this in the context of our CRM, the current
568 work suggests that NGMS could be an important parameter for understanding this phe-
569 nomenon. Furthermore, the WTG approximation could prove to be important for probing
570 this possibility numerically.

571 *Raymond and Sessions* [2007] showed that increasing the atmospheric stability or mois-
572 ture of the reference profile decreases NGMS and increases the precipitation rate for a
573 given set of boundary conditions. Results from that work showed that the highest pre-
574 cipitation rates corresponded to values of NGMS which would be characterized by the
575 dry equilibrium in this work (i.e., $\text{NGMS} < 0.2$). This suggests that the reference profiles
576 also influence the range of boundary conditions which support multiple equilibria. More
577 specifically, this implies that the value of NGMS which separates the two equilibria de-
578 pends on the surrounding environment. Therefore, the dotted line in figure 17 is valid
579 only for a RCE reference profile. We expect that the location of this line will change for
580 different reference profiles.

581 The second observation to make from figure 17 is that, for simulations which sustain
582 convection and precipitation, the precipitation rate increases as NGMS decreases for a
583 given wind speed. The multiple values of rain rate for a given wind speed are a result of
584 the different values of the potential temperature relaxation time scale, t_θ (see discussion in
585 section 3). Furthermore, the precipitation for a given value of NGMS increases with wind
586 speed. The qualitative relationship between precipitation, NGMS and surface fluxes as
587 shown in figure 17 agrees with the steady state condition given by equation (2). Also note
588 that while there is a relationship between NGMS and precipitation within an individual

589 set of simulations, across all sets there is none, except for the split between the two types
590 of equilibrium.

591 The final observation regarding data in figure 17 is that for simulations which resulted in
592 a dry equilibrium, NGMS can be either weakly positive or negative. In all cases, subsidence
593 results in moisture export, and therefore the sign of NGMS in the dry equilibrium is de-
594 termined by whether the moist entropy is imported or exported. Near-surface circulations
595 determine this. Negative values of NGMS have been previously reported in RCE simula-
596 tions by *Bretherton et al.* [2005]. In that work, randomly seeded convection self-organized
597 into a single intensely convecting region surrounded by a dry subsiding atmosphere. The
598 most intensely convecting regions exhibited a positive gross moist stability, while negative
599 values existed elsewhere. Comparing those results to the steady-state NGMS values in
600 our simulations suggests that there is indeed an analogy between the dry and convecting
601 regions in *Bretherton et al.*'s [2005] large RCE domain and our domain-wide dry or moist
602 WTG equilibria (this was also pointed out in SBB07).

603 *Raymond et al.* [2009] also addressed the role of NGMS in the steady state in multiple
604 equilibrium. The authors discussed the idea of having two stable equilibria—one dry and
605 one with persistent deep convection and precipitation—separated by an unstable equilib-
606 rium. Figure 18 is the conceptual picture from *Raymond et al.* [2009], reprinted here
607 for convenience. The existence and location of the unstable equilibrium relative to the
608 stable equilibria is dependent on the boundary conditions. Initial conditions determine
609 the state of the system relative to the unstable equilibrium, and hence which equilibrium
610 is ultimately realized in the steady state.

5. Summary and Discussion

611 We have established the existence of a dry and a precipitating steady state in a cloud
612 resolving model employing the WTG approximation. In this study, we have identified
613 several parameters which control the existence of two equilibrium states: 1) surface fluxes
614 (modulated by SST or surface winds), 2) domain size, and 3) time scale for relaxation
615 of the potential temperature to the environmental mean. Our results suggest that cer-
616 tain combinations of these are necessary for supporting multiple equilibria, and provide
617 some guidance for atmospheric conditions that may also be good candidates for multiple
618 equilibrium states.

619 Given an initially dry environment, the ability of the domain to initiate and sustain deep
620 convection hinges on its capacity to moisten the free troposphere in the face of radiatively
621 induced subsidence and maintain a sufficient saturation fraction. As shown in numerous
622 studies [*Bretherton et al.*, 2004; *Raymond et al.*, 2007], the precipitation is a sensitive
623 function of moisture in the environment, so in order for deep convection to develop,
624 there must be an external source of moisture and a mechanism which serves to transport
625 that moisture into the troposphere. Moisture from the boundary layer is accessible as
626 long as convection can overcome convective inhibition. The most effective channel for
627 this is increasing surface fluxes. Alternatively, some conditions may be conducive to the
628 initiation and development of deep convection, such as regions of low convective inhibition
629 (as occurs with larger domain sizes). Thus, increasing the domain size will increase the
630 likelihood that convection will occur spontaneously and allow the troposphere to tap into
631 the moisture of the boundary layer. In addition to boundary layer moisture, atmospheric
632 circulations can horizontally advect moisture from the surrounding environment, providing

633 an alternate mechanism for the system to transition from the dry state to the precipitating
634 one. This mechanism is likely influenced by the potential temperature relaxation time,
635 t_θ , since this controls the parameterized large-scale vertical motion. By mass continuity,
636 this also affects horizontal flows which may advect moisture. Our results indicate that
637 larger values of t_θ permit the free tropospheric moistening necessary to initiate deep
638 convection. These results are qualitatively consistent with the dependence of multiple
639 equilibria on the moisture relaxation time used in SBB07. In SBB07, longer relaxation
640 times for moisture advection killed the dry equilibrium state. If any of these mechanisms
641 successfully bring the system to the convecting equilibrium from a completely dry state,
642 we assume the conditions are insufficient to sustain a dry equilibrium. Failure, on the
643 other hand, implies the existence of multiple equilibria under the specific set of boundary
644 conditions.

645 It is important to also point out that the dependence on the time scale for relaxation
646 of the local potential temperature profiles to the large scale mean suggests that the weak
647 temperature gradient approximation is an important ingredient in producing multiple
648 equilibria. Our results clearly show that if the WTG approximation is only weakly obeyed
649 (as measured by the magnitude of t_θ), the dry equilibrium is destroyed.

650 Upon establishing a set of boundary conditions capable of supporting multiple equilibria,
651 the actual state realized by the model will depend on the initial moisture in the free
652 troposphere. In this case, there is a threshold fraction of the mixing ratio profile below
653 which the initial moisture is advected out and the system sits at the dry equilibrium.
654 Moisture profiles which exceed the threshold fraction can sustain a convecting equilibrium.
655 The threshold value is a function of boundary conditions, being small for conditions which

656 support heavy precipitation (as with large surface winds) and large in conditions which
657 result in smaller precipitation rates.

658 Finally, we consider NGMS as a diagnostic of environmental characteristics. In the
659 steady state, this set of simulations found that values of NGMS less than 0.25 correspond
660 to the dry equilibrium, while values greater than 0.35 all correspond to a precipitating
661 equilibrium. The dry equilibrium physically represents a region of subsidence where mois-
662 ture is being exported from the domain and there is relatively little exchange of moist
663 entropy between the modeled domain and the surrounding environment, giving rise to
664 the smaller magnitudes of NGMS. Under these conditions, the vertical integral of moist
665 entropy can give a net import or export, depending on circulations in the boundary layer.
666 Completely divergent mass flux profiles imply net entropy export which, when coupled to
667 moisture export, implies a negative value of NGMS in the steady state. Any convergence
668 in the boundary layer is sufficient to import moist entropy and result in a small, positive
669 NGMS.

670 The NGMS also provides insight with respect to transient stages of developing or de-
671 caying deep convection. When convection is developing in an initially dry environment,
672 the domain goes from having a net export of moisture to a net import. Furthermore, the
673 moist entropy convergence of the dry state transitions to a net divergence in the mature
674 stages of convection. As these sign changes need not occur simultaneously, there may be
675 a period of time when both moisture and moist entropy are being imported, resulting in a
676 negative value of NGMS. A similar argument holds also for decaying convection, in which
677 case the period of negative NGMS corresponds to both quantities being exported.

678 **Acknowledgments.** This research was supported in part by the state of New Mexico
679 through resources provided by the New Mexico Computing Applications Center. This
680 work was also supported by U.S. National Science Foundation Grants ATM-0638801 and
681 ATM-0542736.

Notes

1. The actual model input is a fractional multiplier, f_θ , which corresponds to $\delta\theta^{max} = f_\theta\theta_0$. $\delta\theta^{max}$ is approximated here
by multiplying f_θ by 300 K.
682
2. A table of model parameters, including run times of each simulation is provided as a supplement for this paper. It can
also be found at <http://www.physics.nmt.edu/~sessions>
3. The data in figure 15 have been low-pass filtered with a cutoff period of one day. The precipitation rate is calculated as a
time derivative of the cumulative precipitation in the domain. The initial precipitation rate is artificially high since it is
near an end point in the centered difference scheme used in the derivative calculation. This does not affect the calculation
of NGMS.
4. Wind speeds less than 5 ms^{-1} are not expected to sustain convection; however some convection remained in the 50 km
domain with 1 km grid resolution. We are not sure why this happens, but it also causes large fluctuations in NGMS due
to the fluctuations between moisture import and export. Consequently, we also exclude these values of NGMS.

References

- 683 Back, L. E., and C. S. Bretherton (2006), Geographic variability in the export of moist
684 static energy and vertical motion profiles in the tropical Pacific, *Geophys. Res. Letters*,
685 *33*, L17810, DOI: 10.1029/2006GL026672.
- 686 Bellon, G. and A. H. Sobel (2009), Multiple equilibria of the Hadley circulation in an
687 intermediate-complexity axisymmetric model, *J. Climate*, in review.
- 688 Bretherton, C. S. and P. K. Smolarkiewicz (1989), Gravity Waves, Compensating Subsidi-
689 dence and Detrainment around Cumulus Clouds, *J. Atmos. Sci.*, *46*, 740-759.
- 690 Bretherton, C. S., M. E. Peters, and L. E. Back (2004), Relationships between water
691 vapor path and precipitation over the tropical oceans, *J. Climate*, *17*, 1517-1528.

- 692 Bretherton, C. S., P. N. Blossey, and M. Khairoutdinov (2005), An Energy-Balance Anal-
693 ysis of Deep Convective Self-Aggregation above Uniform SST, *J. Atmos. Sci.*, *62*, 4273-
694 4292.
- 695 López-Carrillo, C., and D. J. Raymond (2005), Moisture Tendency Equations in a Tropical
696 Atmosphere, *J. Atmos. Sci.*, *62*, 1601-1613.
- 697 Mapes, B. E. and R. H. Houze Jr. (1995), Diabatic Divergence Profiles in Western Pacific
698 Mesoscale Convective Systems, *J. Atmos. Sci.*, *52*, 1807-1828.
- 699 Neelin, J. D. and I. M. Held (1987), Modeling tropical convergence based on the moist
700 static energy budget, *Mon. Wea. Rev.*, *115*, 3-12.
- 701 Neelin, J. D., O. Peters, and K. Hales (2009), The transition to strong convection, *J.*
702 *Atmos. Sci.*, *66*, 1665-1683, DOI:10.1175/2008JAS2806.1.
- 703 Peters, O., and J. D. Neelin (2006), Critical phenomena in atmospheric precipitation,
704 *Nature Physics*, *2*, 393-396, doi:10.1038/nphys314.
- 705 Raymond, D. J. (2000), Thermodynamic control of tropical rainfall, *Quart. J. Roy. Me-*
706 *teor. Soc.*, *126*, 889-898.
- 707 Raymond, D. J., and A. M. Blyth (1986), A stochastic mixing model for nonprecipitating
708 cumulus clouds, *J. Atmos. Sci.*, *43*, 2708-2718.
- 709 Raymond, D. J., and S. L. Sessions (2007), Evolution of convection during tropical cyclo-
710 genesis, *Geophys. Res. Letters*, *34*, L06811, DOI:10.1029/2006GL028607.
- 711 Raymond, D. J., and X. Zeng (2000), Instability and large scale circulations in a two-
712 column model of the tropical troposphere, *Quart. J. Roy. Meteor. Soc.*, *126*, 3117-3135.
- 713 Raymond, D. J., and X. Zeng (2005), Modelling tropical atmospheric convection in the
714 context of the weak temperature gradient approximation, *Quart. J. Roy. Meteor. Soc.*,

715 131, 1301-1320.

716 Raymond, D. J., G. B. Raga, C. S. Bretherton, J. Molinari, C. López-Carrillo, and Ž. Fuchs
717 (2003), Convective forcing in the intertropical convergence zone of the east Pacific, *J.*
718 *Atmos. Sci.*, 60, 2064-2082.

719 Raymond, D. J., S. L. Sessions and Ž. Fuchs (2007), A theory for the spinup of tropical
720 depressions, *Quart. J. Roy. Meteor. Soc.*, 133, 1743-1754.

721 Raymond, D. J., S. L. Sessions, A. H. Sobel, and Ž. Fuchs (2009), The me-
722 chanics of gross moist stability, *J. Adv. Model Earth Syst.*, 1, Art #9, 20 pp.,
723 doi:10.3894/JAMES.2009.1.9.

724 Sobel, A. H. (2007), Simple models of ensemble-averaged tropical precipitation and surface
725 wind, given the sea surface temperature, in *The Global Circulation of the Atmosphere*,
726 edited by T. Schneider and A. H. Sobel, pp. 219-251, Princeton University Press, New
727 Jersey.

728 Sobel, A. H., and G. Bellon (2008), The effect of imposed drying on parameterized deep
729 convection, *J. Atmos. Sci.*, 66, 2085-2096.

730 Sobel, A. H., and C. S. Bretherton (2000), Modeling tropical precipitation in a single
731 column, *J. Climate*, 13, 4378-4392.

732 Sobel, A. H., G. Bellon, and J. Bacmeister (2007), Multiple equilibria in
733 a single-column model of the tropical atmosphere, *Geophys. Res. Lett.*, 34,
734 L22804,doi:1029/2007GL031320.

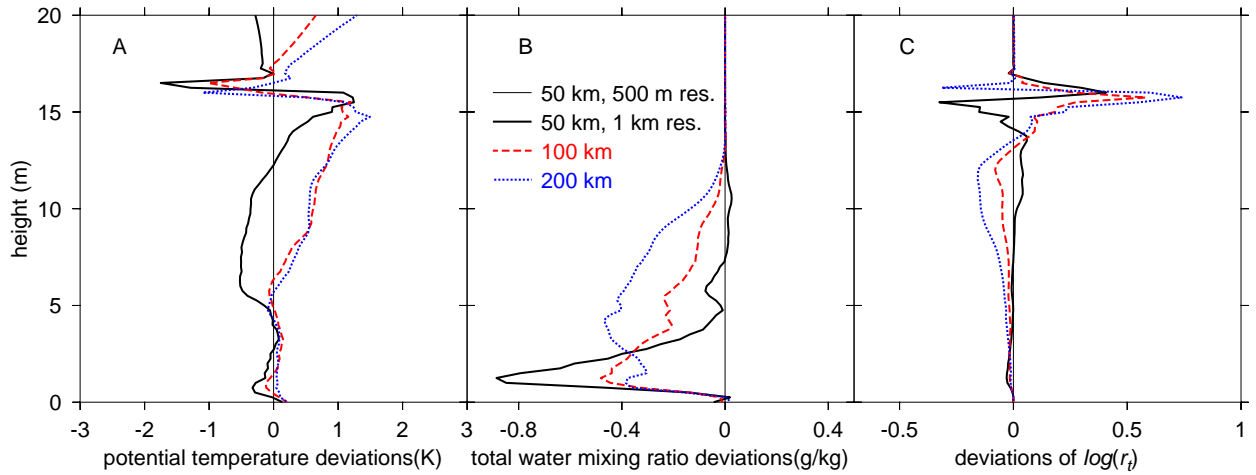


Figure 1. Comparison of RCE profiles for 50, 100, and 200 km domains (solid, dashed, and dotted lines, resp.). To emphasize the difference between the profiles characterizing the large scale environment, we plot the deviations of the profiles from those of the 50 km domain with 500 m resolution (thin solid line). A) Shows deviations in potential temperature, B) gives deviations in total water mixing ratio, and C) shows the differences in the log of the mixing ratio to emphasize the differences in moisture in the upper troposphere. The larger domains are warmer in the upper troposphere, but are also considerably drier. Note the difference in moisture distribution for the 50 km domains (line thickness denotes grid resolution).

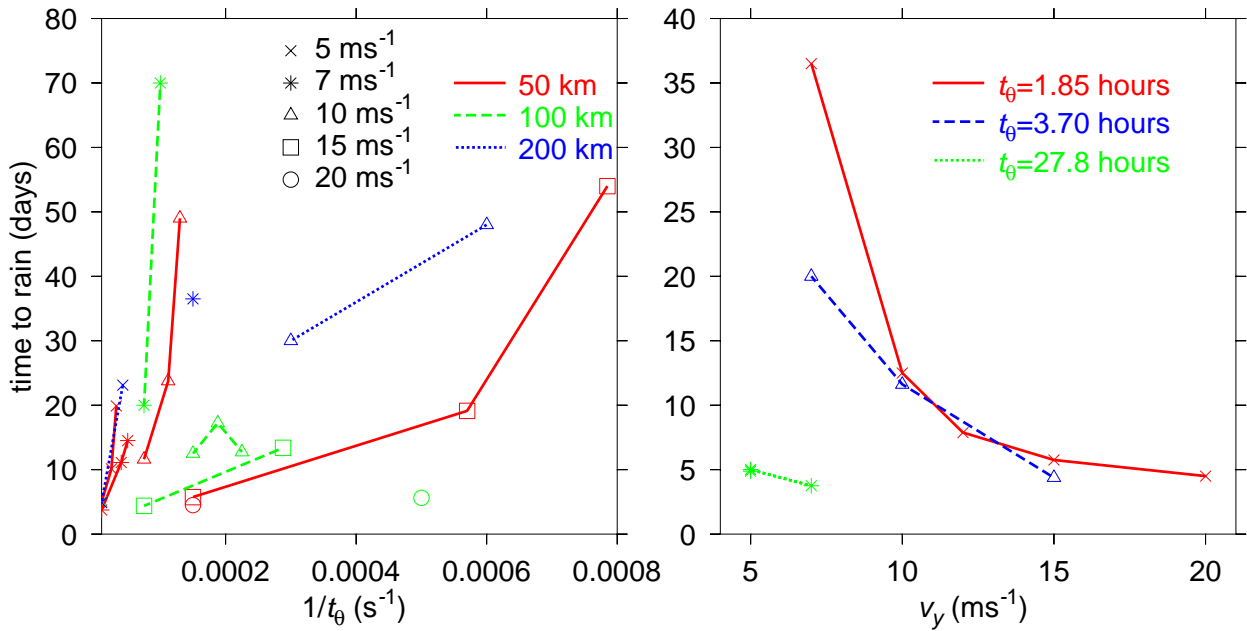


Figure 2. The amount of time needed for an initially dry domain to generate at least 1 mm day⁻¹ precipitation rate is plotted as a function of relaxation rate (t_{θ}^{-1} , left) and surface wind speed (v_y , right). In the first case, lines connect experiments with same domain size (indicated by line style) and wind speed (symbols). Experiments shown on the right panel had a common t_{θ} and thus allowed us to see how the imposed wind speed influenced the onset of precipitation (independent of domain size). Note the different scale on the vertical axes.

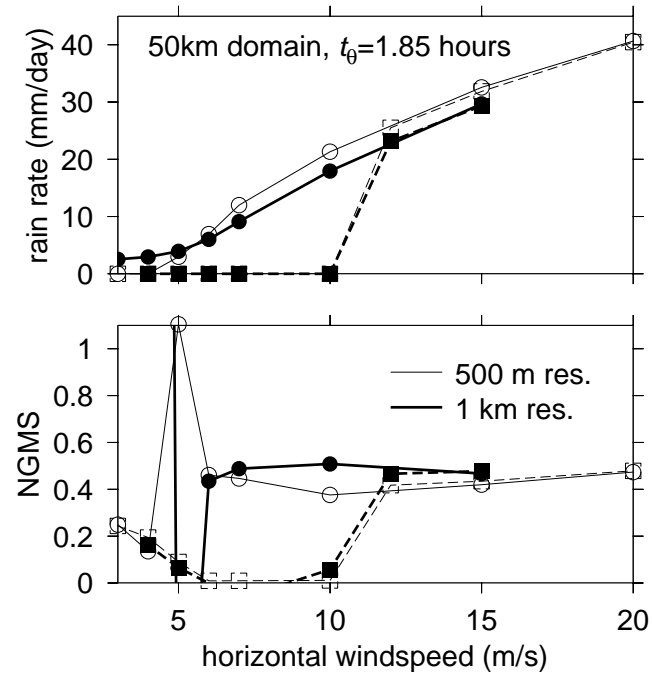


Figure 3. Precipitation (top) and NGMS (bottom) as a function of imposed horizontal wind speed. Solid lines (circles) represent simulations initiated with RCE profiles of potential temperature and mixing ratio. Simulations which were initially dry are shown with dashed lines (squares). Line thickness indicates horizontal grid resolution. In the range of 5 and 10 ms^{-1} , 2 equilibrium states exist regardless of grid resolution; above 10 ms^{-1} , only the precipitating state exists; below 5 ms^{-1} , only the dry state remains for the finer grid, while multiple equilibria persist at lower wind speeds for the coarser grid.

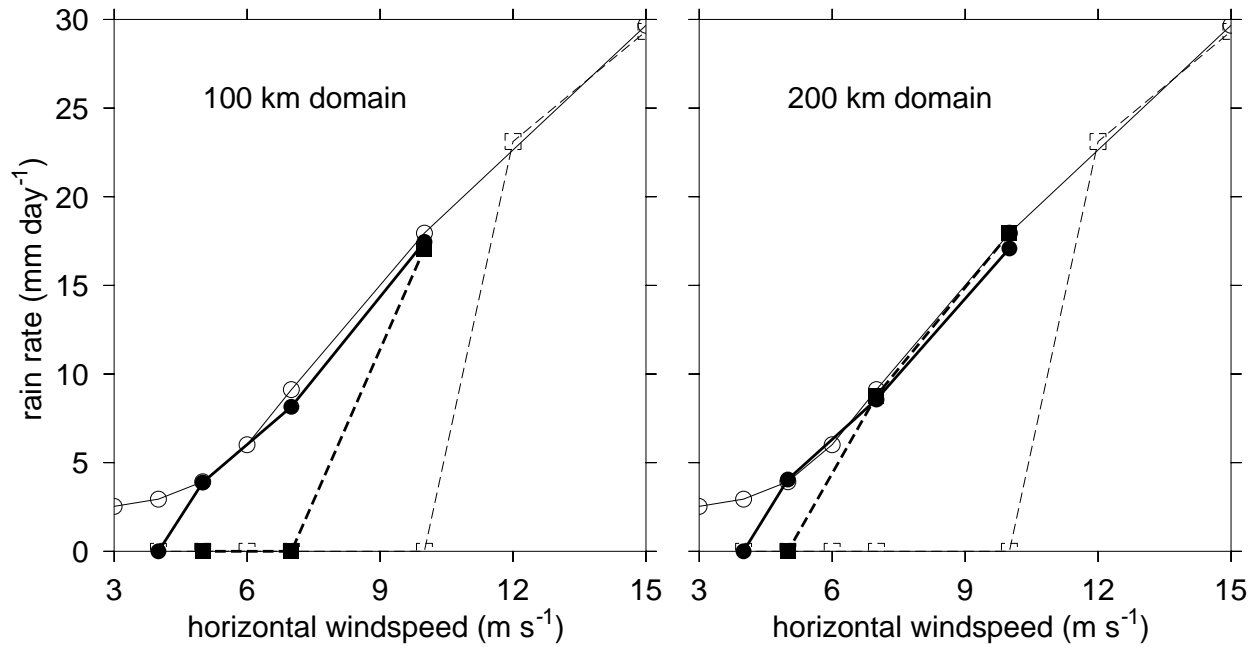


Figure 4. Same as figure 3, but for the 100 and 200 km domain experiments (left and right, respectively). The results for the 50 km domain with 1 km horizontal grid resolution have been overlaid with thin lines and open symbols for comparison. Note that the range wind speeds where multiple equilibria exist decreases as the domain size increases.

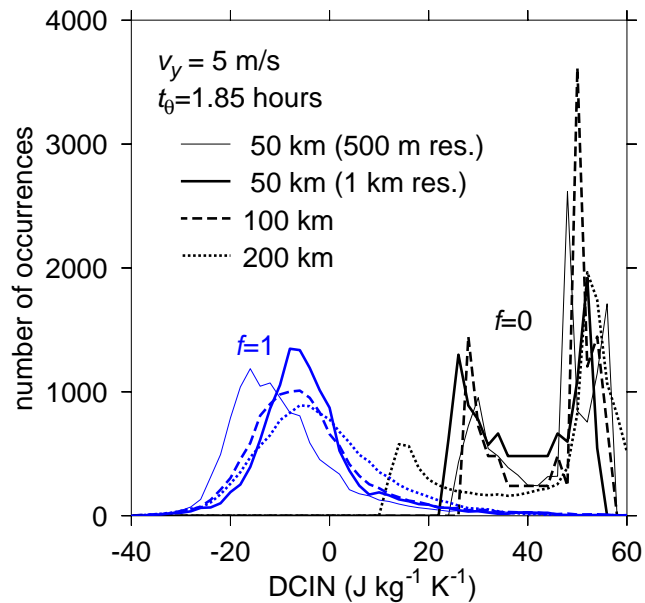


Figure 5. A histogram of values of DCIN (see text) for experiments with surface winds of 5 ms^{-1} and $t_\theta = 1.85 \text{ hours}$. Line styles differentiate domain sizes and resolution. For these boundary conditions, all simulations which were initially dry remained dry ($f = 0$, on the right), and runs initially moist sustained convection ($f = 1$, on the left). Note that the $f = 0$ curve for the 200 km domain has a considerable number of low-DCIN points compared the the other domains.

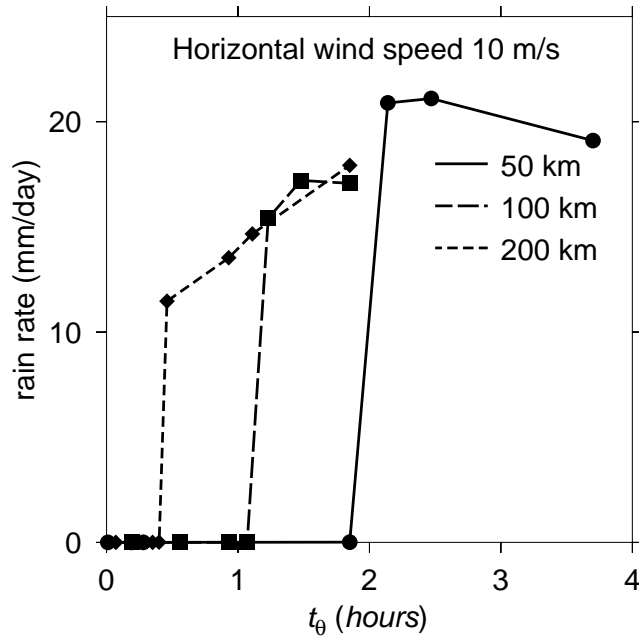


Figure 6. Equilibrium precipitation as a function of potential temperature relaxation time, t_θ , for 50, 100, and 200 km domains. The horizontal imposed wind is 10 ms^{-1} . Symbols represent numerical experiments, all of which are initially dry.

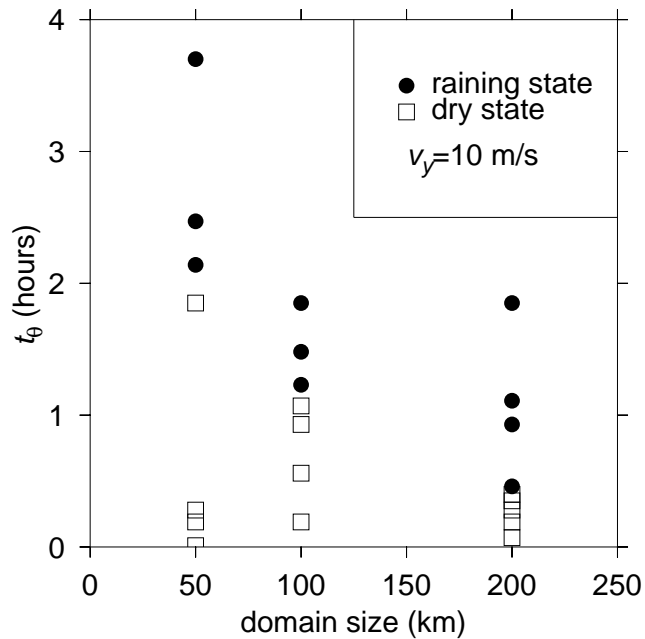


Figure 7. All symbols correspond to simulations initiated with a dry moisture profile and with fixed surface wind speeds (v_y) of 10 ms^{-1} . Solid circles represent experiments that eventually precipitated, open squares represent experiments which remained dry.

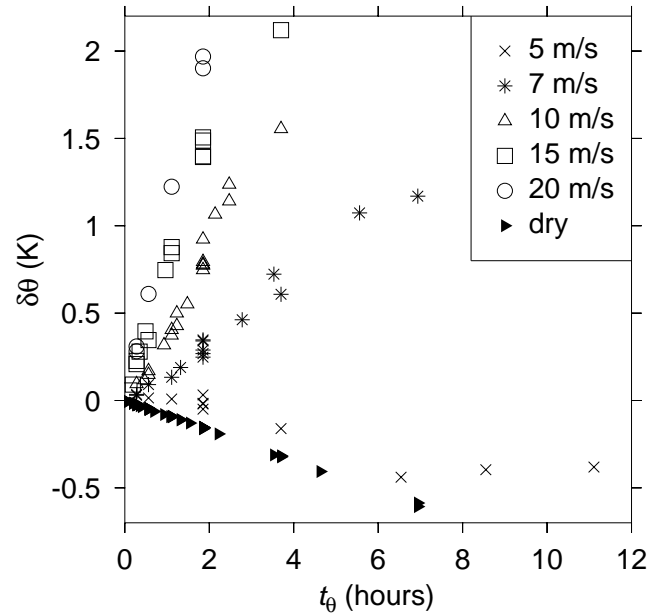


Figure 8. $\delta\theta$ is the time and domain averaged deviation of potential temperature from RCE averaged over 4-12 km in height. In this range, $\delta\theta$ is nearly constant. Black filled triangles represent experiments which resulted in the dry equilibrium, while all other symbols correspond to experiments which evolved to the precipitating equilibrium, independent of initial moisture. For the precipitating states, the different symbols indicate the magnitude of the surface winds. For a given wind speed, the relationship between $\delta\theta$ and t_θ is nearly linear. There is also a linear relation for the non-precipitating states.

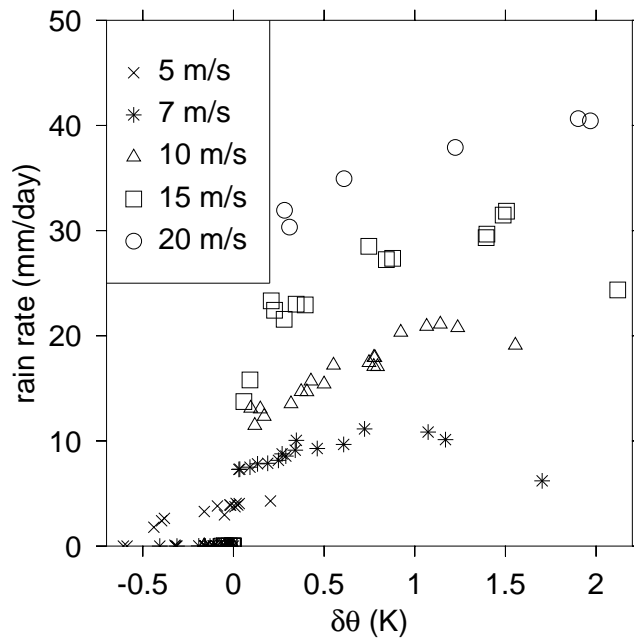


Figure 9. Precipitation rate as a function of $\delta\theta$, with the same key as in figure 8. Non-precipitating equilibrium states are obvious and thus have not been separately identified.

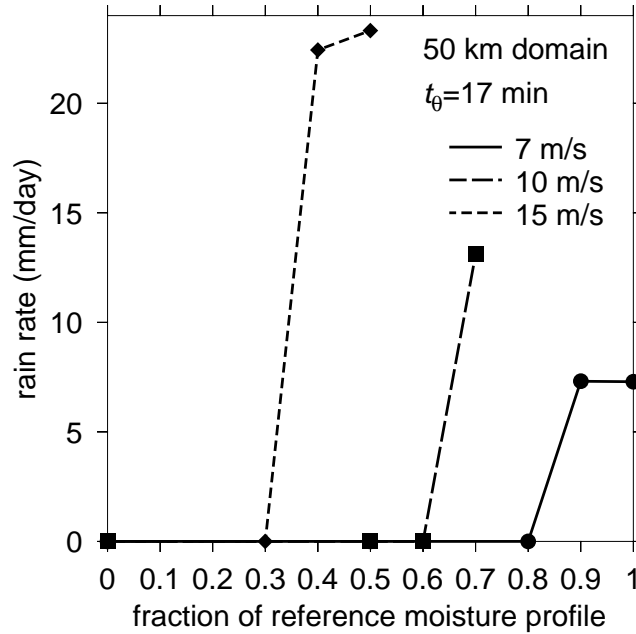


Figure 10. All symbols correspond to simulations on a 50 km domain with $t_\theta = 17$ min. Symbols and line styles represent the sustained surface wind speeds, and the location of the bullets indicate the fraction of the RCE mixing ratio profile which was used to initiate the simulation (i.e., f in equation (3)). Here we see that in some cases, the dry state is maintained even with considerable initial moistening of the free troposphere.

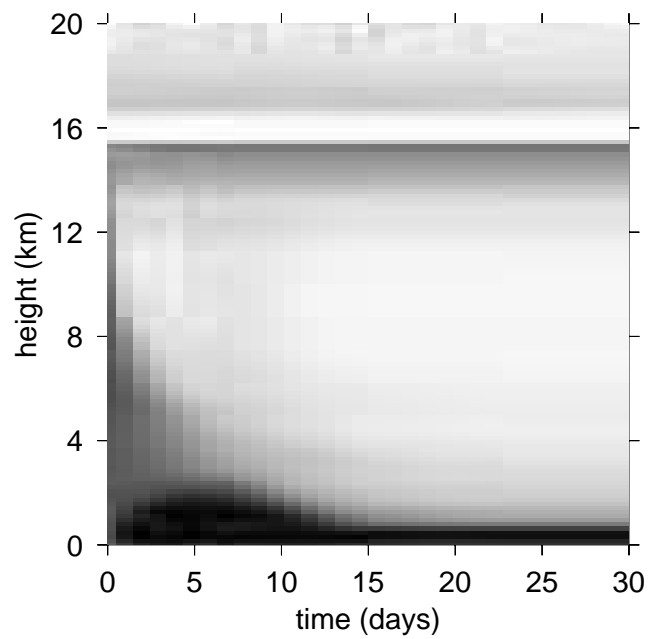


Figure 11. Image plot of the relative humidity. White indicates zero, while black indicates unity. The initial moisture in the free troposphere is removed by subsidence and implied lateral export, resulting in a dry steady state.

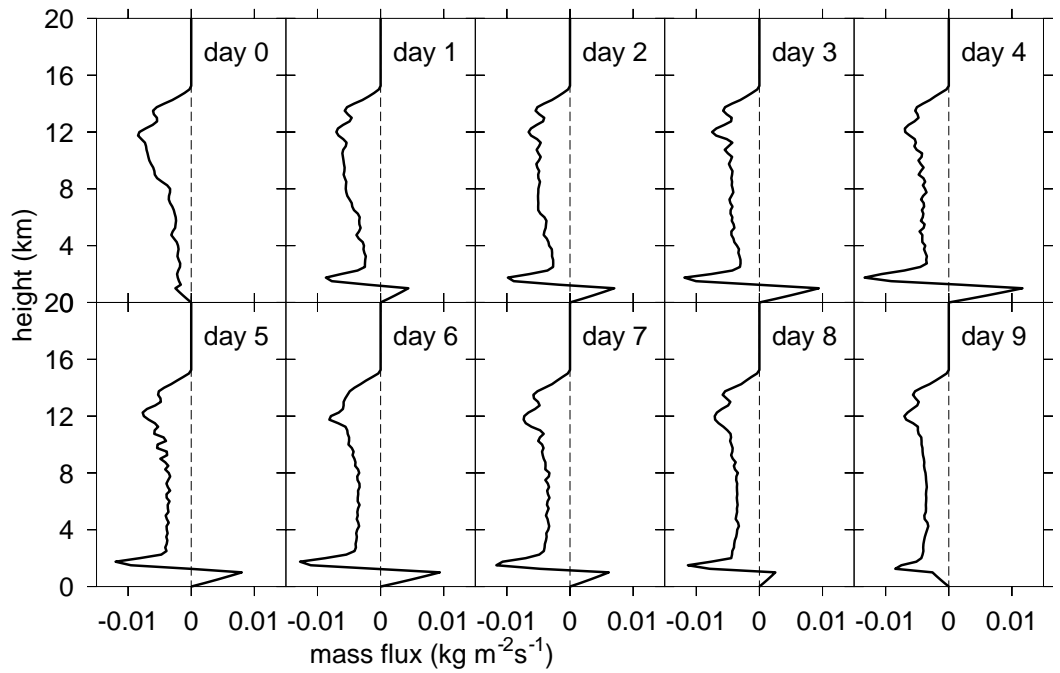


Figure 12. The vertical mass flux profile for the first 10 days of the simulation initiated with 80% of the RCE moisture profile (50 km domain, surface wind speed 7 ms^{-1} , and $t_{\theta}=17 \text{ min.}$). The mass flux profile changes very little in the time after day 9.

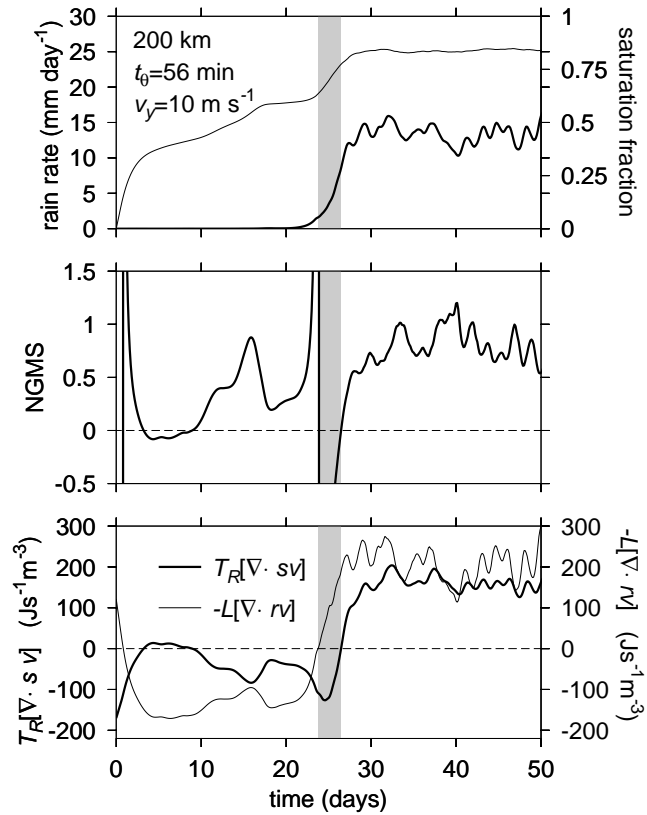


Figure 13. Top: Precipitation rate (thick) and saturation fraction (thin) as a function of time. Middle: NGMS. Bottom: Moist entropy divergence (thick) and moisture convergence (thin). Initiated with a dry atmosphere. The transition period with negative NGMS (days 24-26) is emphasized with grey shading. See text for discussion. Data shown has been low-pass filtered in time with a cutoff period of one day.

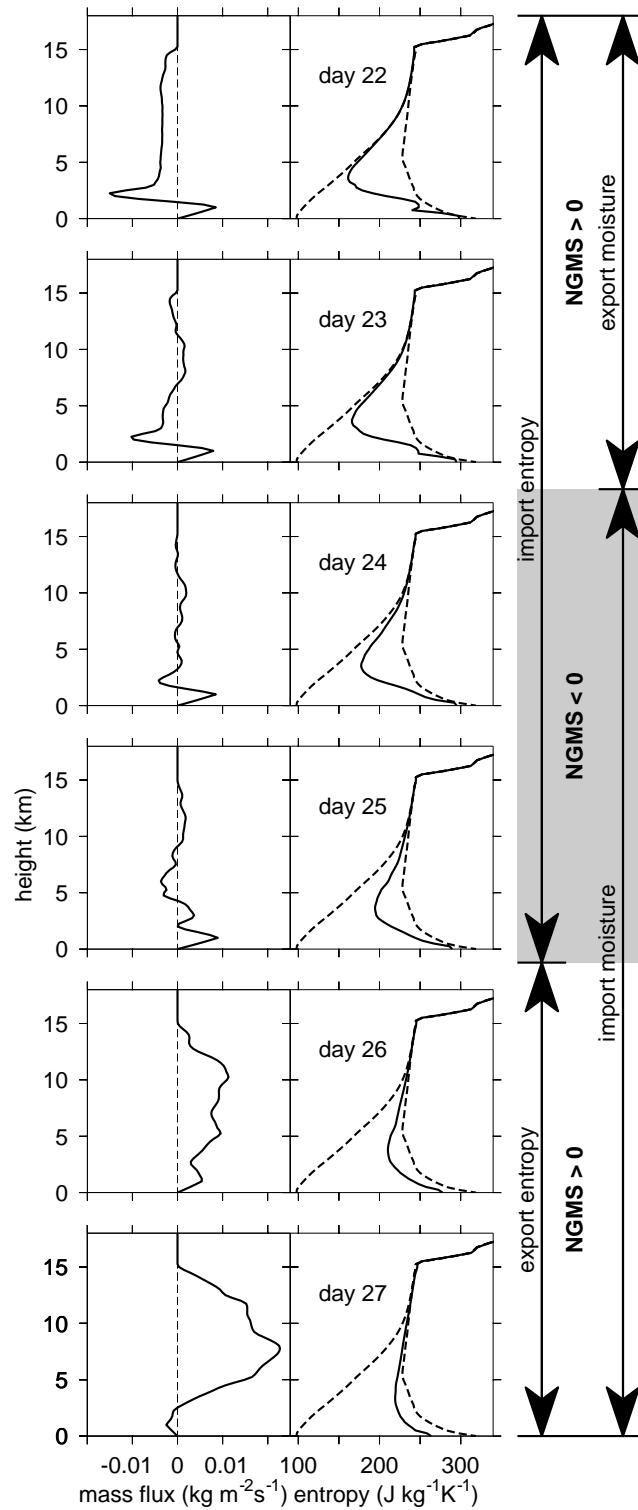


Figure 14. Vertical mass flux profiles (left) and moist entropy (right) for days 22-27 of the simulation shown in figure 13. Dotted lines in the entropy panel are the dry (left) and saturated (right) entropy profiles averaged over days 22-27. Days 24-25 represent time periods where the NGMS is negative. Note the rapid transition in moist entropy during this time.

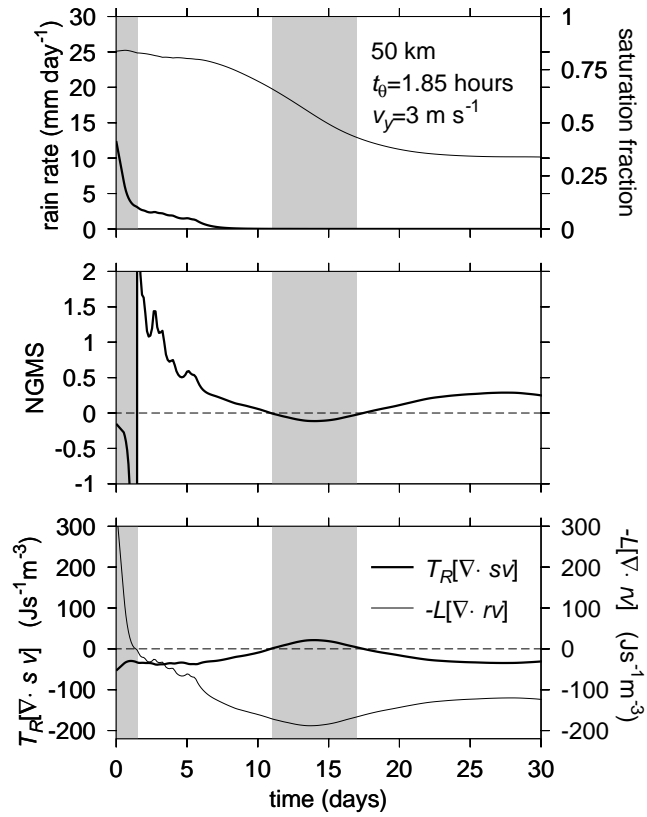


Figure 15. Top: Precipitation rate (thick) and saturation fraction (thin) as a function of time. Middle: NGMS. Bottom: Moist entropy divergence (thick) and moisture convergence (thin). Initiated with moisture profile of surrounding atmosphere. See text for discussion.

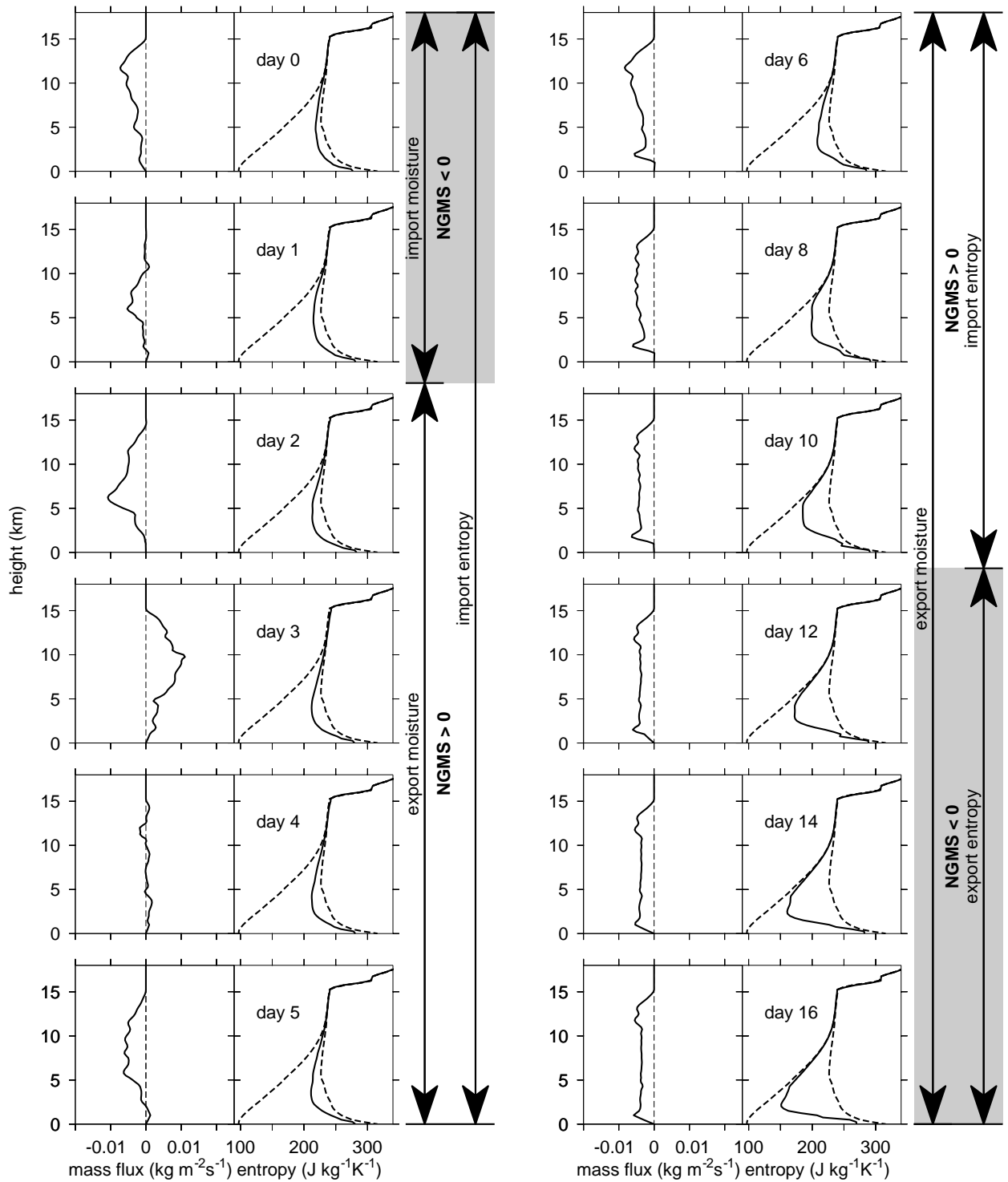


Figure 16. Vertical mass flux profiles (left) and moist entropy (right) for days 0-16 of the simulation shown in figure 15. Dotted lines in the entropy panel are the dry (left) and saturated (right) entropy profiles averaged over days 0-16. Grey shaded regions emphasize the time periods where the NGMS is negative.

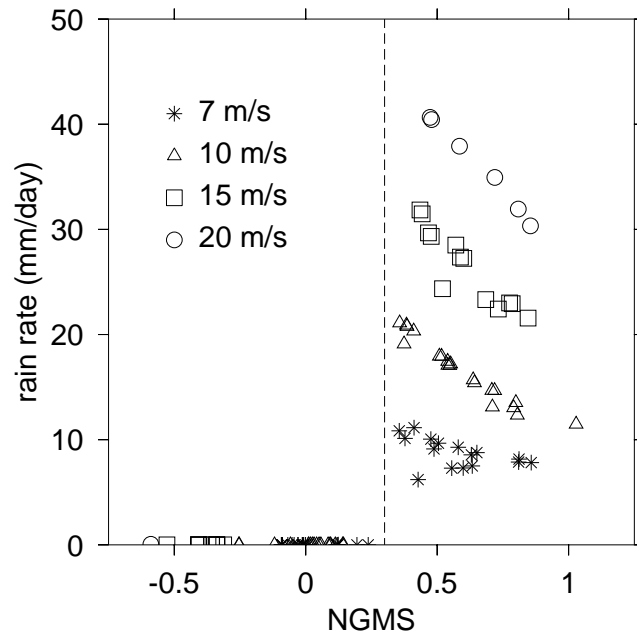


Figure 17. Symbols show the steady state rain rate and NGMS for numerical experiments with prescribed surface winds greater than 5 ms^{-1} . The different symbols represent the strength of the surface winds. A vertical line at $\Gamma = 0.3$ clearly separates the experiments with a dry equilibrium (zero precipitation) from the precipitating equilibrium (precipitation greater than zero).

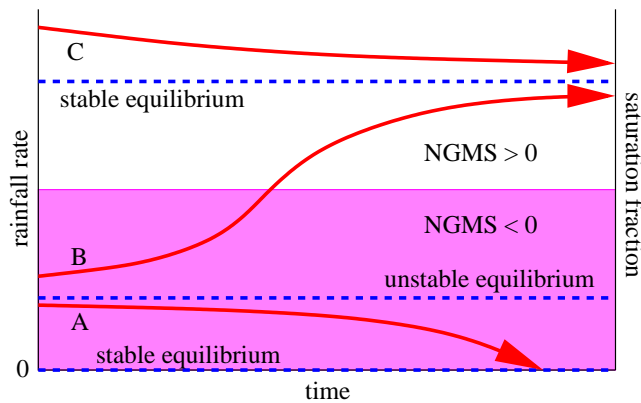


Figure 18. Two stable equilibria, one representing a precipitating state with $\text{NGMS} > 0$, and one with zero precipitation and $\text{NGMS} < 0$. An unstable equilibrium separates these two, and the state ultimately realized by the system will depend on the initial conditions. Previously published as figure 8 in *Raymond et al.* [2009].